Journal of Applied Physics

Joule heat generation in thermionic cathodes of high-pressure arc discharges

Cite as: J. Appl. Phys. **113**, 063301 (2013); https://doi.org/10.1063/1.4790709
Submitted: 26 November 2012 • Accepted: 23 January 2013 • Published Online: 08 February 2013

M. S. Benilov and M. D. Cunha

AIP Publishing

JOURNAL OF APPLIED PHYSICS **113**, 063301 (2013)

Joule heat generation in thermionic cathodes of high-pressure arc discharges

M. S. Benilov and M. D. Cunha
Departamento de Física, CCCEE, Universidade da Madeira, Largo do Município, 9000 Funchal, Portugal

(Received 26 November 2012; accepted 23 January 2013; published online 8 February 2013)

The nonlinear surface heating model of plasma-cathode interaction in high-pressure arcs is extended to take into account the Joule effect inside the cathode body. Calculation results are given for different modes of current transfer to tungsten cathodes of different configurations in argon plasmas of atmospheric or higher pressures. Special attention is paid to analysis of energy balances of the cathode and the near-cathode plasma layer. In all the cases, the variation of potential inside the cathode is much smaller than the near-cathode voltage drop. However, this variation can be comparable to the volt equivalent of the energy flux from the plasma to the cathode and then the Joule effect is essential. Such is the case of the diffuse and mixed modes on rod cathodes at high currents, where the Joule heating causes a dramatic change of thermal and electrical regimes of the cathode. The Joule heating has virtually no effect over characteristics of spots on rod and infinite planar cathodes. © *2013 American Institute of Physics*. [http://dx.doi.org/10.1063/1.4790709]

I. INTRODUCTION

Considerable advances have been attained during the last decade in the theory and modeling of plasma-cathode interaction in high-pressure arc discharges; e.g., review Ref. 1 and references therein. In particular, available simulation methods allow one to self-consistently compute distributions of temperature and electric current density over the cathode surface in cases where the current transfer occurs both in the diffuse and spot modes.

There is, however, an important aspect that is not clear enough up to now: the effect of Joule heat generation in the cathode body. In most works, this effect was neglected compared to energy flux coming from the plasma. For low currents, this simplification is justified and in fact the insignificance of the Joule heating follows from results of numerical modelling.[2,3]

On the other hand, Joule heating may play a role for high currents. For example, the presence of an off tip maximum in the measured distributions of temperature over the surface of thoriated tungsten cathodes with conical tips with small cone angles[4] was interpreted as an effect produced by a combination of thermal conduction, ohmic heating in the bulk of the cathode, and cooling of the cathode surface in the arc attachment region due to thermionic emission of electrons. Cathode temperature distributions with a maximum positioned off the cathode tip were also observed in the experiments.[5]

Another important question concerns the role of Joule effect in cases where the current transfer occurs in the spot mode with a high current density in the spot. This question and especially the possibility of an instability caused by a positive feedback between the Joule heat production and temperature because of the Wiedemann-Franz law (the so-called thermal runaway) have been extensively discussed for volatile cathodes of vacuum arcs, e.g., Refs. 6–8.

In this work, the effect of Joule heat generation in the cathode body is investigated by means of numerical simulations. Special attention is paid to analysis of energy balances of the cathode and the near-cathode plasma layer. The outline of the paper is as follows. The numerical model is described in Sec. II. Numerical results are given in Sec. III and their discussion in Sec. IV. Conclusions are summarized in Sec. V.

II. THE MODEL

A theoretical model of plasma-cathode interaction in high-pressure arc discharges which exploits the fact that a significant power is deposited by the arc power supply into the near-cathode space-charge sheath is frequently termed the model of nonlinear surface heating. This model has been convincingly validated at low currents typical of high-intensity discharge lamps; e.g., Refs. 1 and 9 and references therein. In recent years, different variants of this model have been used also for high currents typical of arc welding.[10–13] In this work, the model of nonlinear surface heating is written with account of Joule heating, similarly to Refs. 2 and 3. Steady-state distributions of temperature T and electrostatic potential φ in the cathode body are governed by the heat conduction and current continuity equations

$$\nabla \cdot (\kappa \nabla T) + \sigma (\nabla \varphi)^2 = 0, \tag{1}$$

$$\nabla \cdot (\sigma \nabla \varphi) = 0. \tag{2}$$

Here, κ and σ are thermal and electrical conductivities of the cathode material, which are treated as known functions of the local temperature: $\kappa = \kappa(T), \sigma = \sigma(T)$.

Boundary conditions at the part of the cathode surface that is in contact with the plasma and the cold gas (Γ_h) are

$$\kappa \frac{\partial T}{\partial n} = q(T_w, U), \quad \sigma \frac{\partial \varphi}{\partial n} = j(T_w, U), \tag{3}$$

where n is a direction locally orthogonal to the cathode surface and directed from the cathode into the plasma and

q and j are densities of net energy flux and electric current from the plasma to the cathode surface. The latter quantities are determined from a model of the near-cathode plasma layer (e.g., Section 3.2 of Ref. 1) and are treated here as known functions of the local temperature T_w of the cathode surface and of the near-cathode voltage drop U: $q = q(T_w, U)$, $j = j(T_w, U)$. Note that $q = q_p - q_r$, where q_p is the density of plasma-related energy flux to the cathode surface (or, more precisely, the density of net energy flux delivered to the cathode surface by the charged particles; the contribution of neutral atoms is neglected) and q_r is the density of losses of energy by the cathode surface through radiation.

Boundary conditions at the base of the cathode (Γ_c) read

$$T = T_c, \quad \varphi = 0, \tag{4}$$

where T_c is the temperature of the base, which is governed by the external cooling arrangement and is treated as a control parameter.

The arc current I is determined by the distribution of the cathode surface temperature and by the near-cathode voltage drop and is given by the formula

$$I = \int_{\Gamma_h} j(T_w, U)\, dS. \tag{5}$$

I is treated as a given parameter and the near-cathode voltage drop U is a parameter to be found as a part of the solution, along with distributions of the temperature and potential.

Note that the above model neglects changes of the cathode shape due to melting and/or evaporation of the cathode material with subsequent return of a part of the evaporated metal to the cathode in the form of either neutral atoms (condensation of the vapor) or ions (the so-called recycling). These changes take from several minutes to several hours (e.g., Sections 3.2 and 3.4 of Ref. 14 and Section 2 of Ref. 15) and may be considered as frozen on the time scales characteristic for processes in the near-cathode plasma and for heat propagation in the cathode body.

The above-stated problem admits a first integral: the equation of integral balance of energy of the cathode, which may be written as

$$Q_p + Q_J = Q_c + Q_r, \tag{6}$$

where

$$Q_p = \int_{\Gamma_h} q_p\, dS, \quad Q_J = \int_V \sigma(\nabla\varphi)^2\, dV, \tag{7}$$

$$Q_c = \int_{\Gamma_c} \left(-\kappa \frac{\partial T}{\partial n}\right) dS, \quad Q_r = \int_{\Gamma_h} q_r\, dS. \tag{8}$$

(Here, V is the cathode volume.) Note that Q_p is the integral power delivered to the cathode by the plasma, Q_J is the integral power dissipated in the cathode body due to Joule effect, Q_c is the integral power removed by heat conduction from the cathode body to the cooling fluid, and Q_r is the integral power radiated by the cathode surface.

One can write also the equation of integral balance of energy of the near-cathode layer, which has been well known since the work[16] and may be written in the form (Section 3.2 of Ref. 1)

$$IU = Q_p + I(A_f + 3.2kT_e^*)/e. \tag{9}$$

Here, A_f is the work function of the cathode material, k is the Boltzmann constant, T_e^* is a weighted average value of the electron temperature in the near-cathode layer, and e is the electron charge. The lhs of this equation represents the electrical power deposited into the near-cathode layer by the arc power supply, terms on the rhs represent, respectively, the power transported from the near-cathode layer to the cathode and the power transported from the layer into the bulk plasma by the (electron) current. Introducing a volt equivalent of the energy flux from the plasma to the cathode, $U_p = Q_p/I$, and a volt equivalent of the power transported into the bulk plasma, $U_{ent} = (A_f + 3.2kT_e^*)/e$, one may rewrite Eq. (9) as

$$U = U_p + U_{ent}. \tag{10}$$

Numerical results reported in this work refer to cathodes made of pure tungsten or tungsten doped with 2% of thorium and arcs burning in argon under the pressure of 1 bar or somewhat higher. Functions $q_p(T_w, U)$ and $j(T_w, U)$ are evaluated by means of a model of the near-cathode plasma layer described in Ref. 17. Data on thermal conductivity and emissivity of tungsten have been taken from Refs. 18 and 19, respectively. Electrical conductivity of tungsten was evaluated in terms of thermal conductivity with the use of the Wiedemann-Franz law. Note that the data on electrical conductivity obtained in this way deviate from the data recommended by the authors[20] by no more than 24% in the whole temperature range where the recommended data are available (up to 3600 K). The usual value of 4.55 eV was assumed for the work function of pure tungsten. The value of 2.63 eV was assumed for the work function of tungsten doped with 2% of thorium following the work.[21] Numerical solution of the above-described boundary-value problems has been obtained by means of the commercial finite element software COMSOL MULTIPHYSICS.

III. NUMERICAL RESULTS

Calculation results reported in this section refer to tungsten cathodes and argon arcs under the following four sets of conditions, which are typical for experiments with high-pressure arc discharges (e.g., Refs. 15, 22, and 23): (1) plasma pressure $p = 2.6$ bar, cylindrical cathode of radius $R = 0.75$ mm and height $h = 24$ mm, $T_c = 293$ K, current transfer occurs in the diffuse mode; (2) $p = 2.6$ bar, cylindrical cathode, $R = 0.3$ mm, $h = 20$ mm, $T_c = 300$ K, diffuse mode; (3) $p = 1$ bar, cylindrical cathode with a hemispherical tip, $R = 1$ mm, $h = 12$ mm, $T_c = 300$ K, current transfer occurs in a mode which embraces states with a hot spot at low currents and states with a diffuse temperature distribution at high currents (this mode was investigated in Ref. 24 and in the following will be the termed mixed mode); (4)

$p = 2.6$ bar, cylindrical cathode, $R = 0.75$ mm, $h = 20$ mm, $T_c = 300$ K, the spot mode. Also reported are results on a solitary spot on an infinite planar cathode in the atmospheric-pressure plasma.

Note that results of simulations without account of the Joule effect for these variants are reported in Ref. 25 (variant 1), Ref. 26 (variants 2 and 4), Ref. 24 and (variant 3), and Ref. [27 (spot on an infinite planar cathode). Also given in Refs. 24–26 is a comparison of simulations for the first four variants with the experimental data.[15,22,23] This work is concerned with the effect of Joule heating.

A. Diffuse mode

Fig. 1(a) illustrates thermal balance of the cathode for variant 1 in a wide arc current range; here, T_m designates the maximum value of the temperature of the cathode body. One can see that the dependence $T_m(I)$ is growing in the most part of the current range, as could be expected on intuitive grounds. The situation is less trivial for $105\,\text{A} \lesssim I \lesssim 131\,\text{A}$:

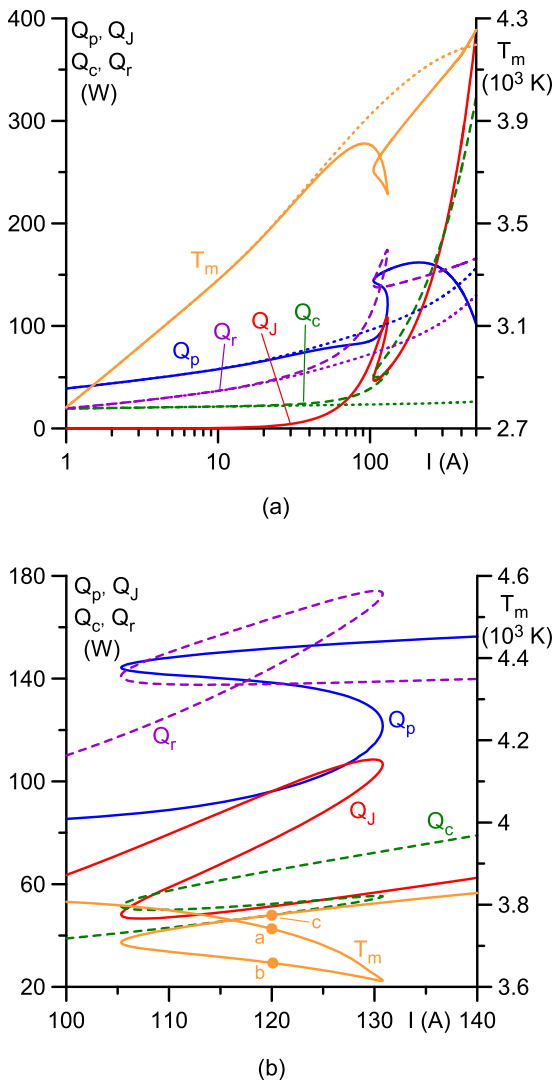

FIG. 1. Thermal balance of the cathode. $p = 2.6$ bar, cylindrical cathode, $R = 0.75$ mm, $h = 24$ mm, $T_c = 293$ K, diffuse mode. Solid and dashed: calculations with account of Joule heat generation. Dotted: calculations neglecting Joule heat generation. Circles: states at the same current of $I = 120$ A.

the curve $T_m(I)$ exhibits a loop in this range. (A magnification of Fig. 1(a) in this range is shown in Fig. 1(b).) In other words, the mode of current transfer being considered possesses two turning points, one at $I \approx 105$A and the other at $I \approx 131$A, and a retrograde section between these turning points. It follows that three different steady-state regimes of current transfer are possible for any current from the range $105\text{A} \lesssim I \lesssim 131\text{A}$.

Modes of current transfer to arc cathodes with retrograde sections have been found in numerical calculations previously, examples being Figures 4(c), 7(c), 7(d), and 9(b) of Ref. 24. Note that the curves $T_m(I)$ shown in the mentioned figures exhibit not a loop but rather Z-shapes, similar to the one exhibited in Fig. 1 by the curve $Q_J(I)$. However, this can hardly be considered as a major difference since both loops and Z-shapes represent a manifestation of the retrograde behavior of the mode. In more general terms, the existence of multiple solutions describing different modes of current transfer to the cathode for the same arc current in models neglecting Joule heating inside the cathode (such as the model[24]) is well known and represents the basis of modern theory of arc plasma-cathode interaction; e.g., review Ref. 1 and references therein. The existence of multiple solutions in such models is a manifestation of non-uniqueness of multidimensional thermal balance of a finite body heated by a nonlinear external energy flux. However, the discharge parameters computed for the present conditions without account of Joule heating inside the cathode and shown in Fig. 1(a) by the dotted lines do not reveal a retrograde section. Hence, the retrograde section under present conditions is related to the Joule heating. In the following, this question will be addressed in some detail.

One can see from Fig. 1(a) that power losses of the cathode due to radiation and thermal conduction, Q_r and Q_c, are close for low currents. When Joule heat generation is not taken into account, Q_c is, roughly speaking, proportional to $(T^* - T_c)$, where T^* is a weighted average value of the temperature of the current-collecting part of the cathode surface. Since the latter does not change much with current, Q_c does not change much as well, and this indeed can be seen in Fig. 1(a). Q_r, being proportional to the fourth power of the temperature, increases in a sizable way. The Joule effect causes a modest increase of Q_r and a quite significant increase of Q_c; Q_c exceeds Q_r for $I \gtrsim 248$A. For higher currents, the ratio Q_c/Q_r continues to increase: most of the power delivered to the cathode by the plasma and dissipated in the cathode due to Joule effect is removed by heat conduction.

The power dissipated in the cathode body due to Joule effect, Q_J, is negligible for low currents. However, Q_J rapidly increases with increasing current: if thermal regime of the cathode and, therefore, its electrical resistance do not change much, then Q_J increases approximately proportionally to I^2. Indeed, analysis of the data shown in Fig. 1(a) reveals that Q_J increases approximately proportionally to I^2 for $I \lesssim 100$A. The Joule heat generation starts producing a sizable effect on characteristics of the discharge from $I \approx 50$A. In particular, the Joule heat generation causes the appearance of the above-discussed retrograde section in the

current range $105\text{A} \lesssim I \lesssim 131\text{A}$. After the retrograde section, Q_J continues to increase with increasing current, although somewhat slower than I^2.

For $I \lesssim 50\text{A}$, the power delivered to the cathode by the plasma, Q_p, is such as required to compensate the cathode power losses $Q_c + Q_r$. At higher currents, the Joule heat generation comes into play and Q_p is no longer governed by the losses: Q_p starts growing slower than $Q_c + Q_r$ and at $I \approx 215\text{A}$ starts decreasing.

For $I \gtrsim 271\text{A}$, Q_J exceeds Q_p, meaning that in this current range the main heating mechanism of the cathode is the Joule effect.

In Fig. 2(a), the current-voltage characteristic (CVC) of the near-cathode layer, $U(I)$, is shown, along with the cathode heating voltage U_p, the volt equivalent U_{ent} of the power transported into the bulk plasma, the volt equivalent $U_J = Q_J/I$ of the heat produced due to the Joule effect, and the maximum value φ_m of the potential in the cathode body. Fig. 2(b) is a magnification of Fig. 2(a) in the current range

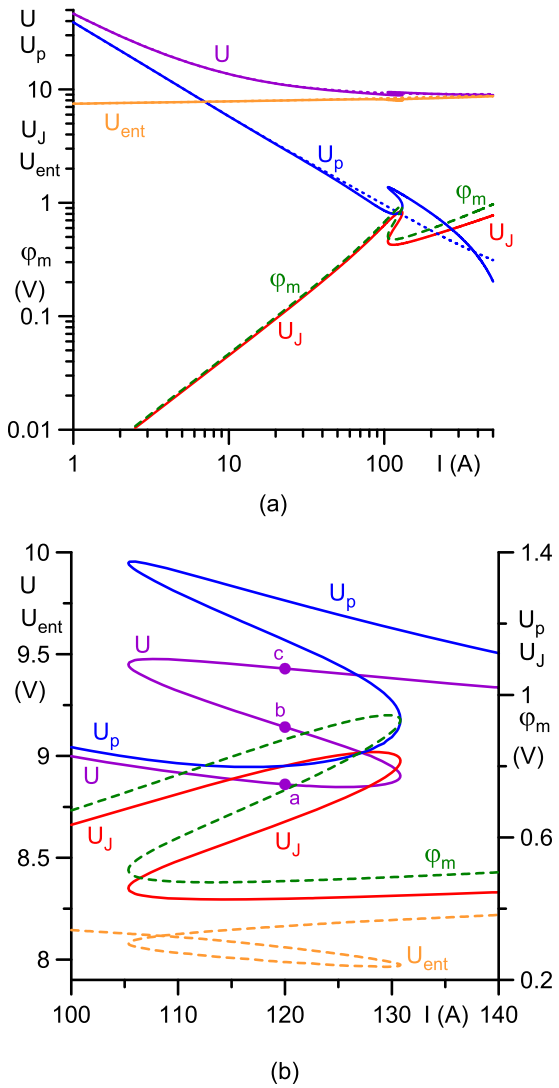

FIG. 2. Energy balance of the near-cathode layer, maximum voltage drop inside the cathode, and volt equivalent of the Joule heating. $p = 2.6$ bar, cylindrical cathode, $R = 0.75$ mm, $h = 24$ mm, $T_c = 293$ K, diffuse mode. Dotted: calculations neglecting Joule heat generation. Circles: states at the same current $I = 120$ A.

where the retrograde behavior occurs. Also present in Fig. 2(a) are dotted lines representing U, U_p, and U_{ent} evaluated without account of the Joule heating; however, they coincide with the solid lines except for U_p at high currents.

At low currents, U_p exceeds U_{ent}: most, or even virtually all, of the energy deposited by the external circuit into the near-cathode layer is transported to the cathode. With increasing current, U_p decreases, in accord with the above-described behavior of Q_p, while U_{ent} does not change much. Starting from $I \approx 7\text{A}$, U_{ent} exceeds U_p: most, or even virtually all, of the energy deposited into the near-cathode layer is transported into the bulk plasma.

The maximum value of potential in all the cases is attained at the surface of the cathode and is in the range of millivolts for currents of one or several amperes and about 1 V at high currents. It follows that φ_m, while being at high current sufficient to produce significant Joule heating, is still much smaller than U. The Joule heating voltage, U_J, is close to the maximum voltage drop inside the cathode, φ_m. This can be understood as follows: multiplying Eq. (2) by φ and integrating over the cathode body one can show that $U_J = \frac{1}{I}\int_{\Gamma_h} \varphi\, j(T_w, U)\, dS$; the rhs of this expression is close to φ_m provided that the potential of the cathode surface within the arc attachment is close to φ_m. The latter is indeed the case, as attested by distributions of potential and current density along the cathode surface shown in Fig. 3. (In this figure, d is the distance from the centre of the front surface of the cathode measured along the generatrix; the range $0 \le d \le 0.75$mm corresponds to the front surface of the cathode while the range $d \ge 0.75$mm corresponds to the lateral surface.)

Also shown in Fig. 3 are distributions of the surface temperature. For $I = 10$ A, maximum values of the surface temperature and current density are attained at the edge of the front surface of the cathode. Such distributions are typical for the diffuse mode without Joule heating at low currents;[25] indeed, the distributions for $I = 10$ A coincide to the graphic accuracy with those calculated without account of the Joule heating. In the model without Joule heating, the

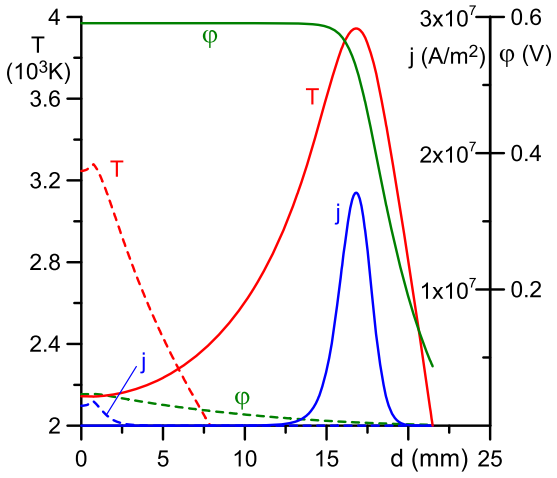

FIG. 3. Distributions of the potential, the current density, and the temperature along the cathode surface. $p = 2.6$ bar, cylindrical cathode, $R = 0.75$ mm, $h = 24$ mm, $T_c = 293$K, diffuse mode. $I = 10$ A (dashed), 200 A (solid).

maxima are flattened for high currents and the entire front surface of the cathode and the adjacent part of the lateral surface become uniformly hot.[27] The account of Joule heating changes this pattern, as shown by the distributions for $I = 200$ A: with increasing current, the maxima of the surface temperature and the current density are shifted in the direction to the base of the cathode. The maxima become very well pronounced while the front surface of the cathode becomes rather cold and collects no current.

The above-described variation of the thermal regime of the cathode occurs on the retrograde section, as shown by Fig. 4. In spite of the current range where the retrograde behavior occurs being relatively narrow, the variation is dramatic: while in the state a the hottest part of the cathode is the front surface and the adjacent section of the lateral surface, there is a well pronounced maximum on the lateral surface at about half the cathode height in the state c. At state b, the thermal regime of the cathode is intermediate. Also shown in Fig. 4 is the temperature distribution calculated for the same current $I = 120$ A without account of the Joule heating. One can see that the effect of the Joule heating is considerable already in the state a.

Note that the absolute maximum of the temperature of the cathode body (to which the data shown in Fig. 1 refer) occurs on the surface for currents below approximately 400 A. At higher currents, the absolute maximum occurs on the cathode axis; however, T_m exceeds the highest temperature on the surface by no more than 30 K even in such situations.

An important question is which of the three steady-state solutions that exist in the current range $105\text{A} \lesssim I \lesssim 131\text{A}$ are stable and can be observed in the experiment. Numerical simulations with the non-stationary term being added to the heat-conduction equation, Eq. (1), have been performed in order to answer this question. It was found that states belonging to the retrograde section are unstable and states outside the retrograde section are stable, which is a usual situation.

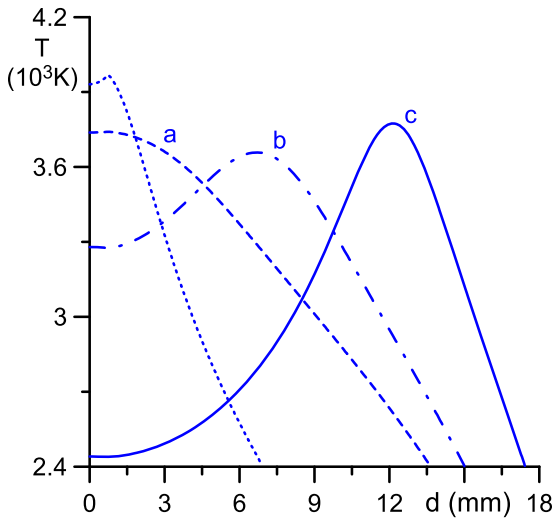

FIG. 4. Distributions of the temperature along the cathode surface. $p = 2.6$ bar, cylindrical cathode, $R = 0.75$ mm, $h = 24$ mm, $T_c = 293$K, diffuse mode. $I = 120$ A, states a, b, and c are indicated in Figs. 1(b) and 2(b). Dotted: calculation for $I = 120$ A without account of Joule heat generation.

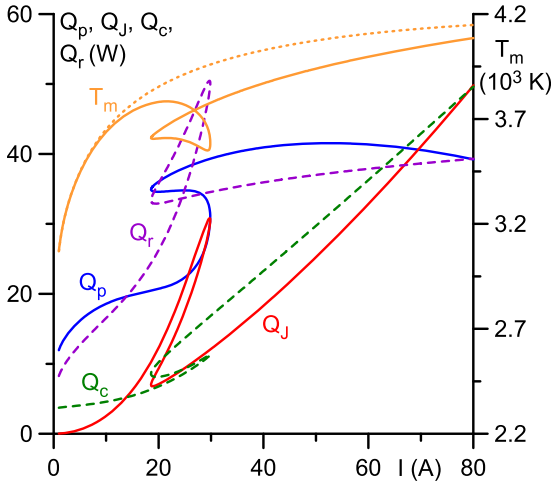

FIG. 5. Thermal balance of the cathode. $p = 2.6$ bar, cylindrical cathode, $R = 0.3$ mm, $h = 20$ mm, $T_c = 300$ K, diffuse mode. Dotted: calculations neglecting Joule heat generation.

In other words, states a and c in Figs. 1(b) and 2(b) are stable and state b unstable. Therefore, the mode being considered manifests hysteresis. In principle, the hysteresis can be observed in the experiment, although in a narrow current range.

The above data refer to the conditions of variant 1. Fig. 5 illustrates the thermal balance of the cathode for variant 2, which differs mostly by a significantly smaller cathode radius. The figure is qualitatively similar to Fig. 1(a), the main difference being that the Joule effect comes into play and the retrograde behavior occurs at significantly lower currents. The Joule effect is the main heating mechanism of the cathode, i.e., $Q_J > Q_p$, for $I \gtrsim 70$A.

B. Mixed mode

In Fig. 6, characteristics of the plasma-cathode interaction are shown for variant 3. We remind that this variant differs from variant 1 by a bigger cathode radius, a significantly smaller cathode height, and the cathode tip being hemispherical; the mode of current transfer occurring in these conditions was investigated in Ref. 24, embraces states with a hot spot at low currents and states with a diffuse temperature distribution at high currents, and is termed here mixed mode. Figs. 6(a) and 6(b) are qualitatively similar to Figs. 1(a) and 2(a), the main difference being that the retrograde behavior in Fig. 6 occurs at low currents, where the Joule heating produces virtually no effect. In fact, this behavior is typical of the mixed mode of current transfer:[24] it is associated with a transition between states with a narrow current spot and diffuse-like states with a wide attachment. Again, non-stationary simulations revealed that states belonging to the retrograde section are unstable and states outside the retrograde section are stable, so the mode manifests hysteresis which, in principle, can be observed in the experiment. The Joule effect comes into play at currents around 100 A without a retrograde behavior. Again, the Joule heating results in a decrease of the temperature of the hottest point of the cathode and there is a current range where the dependence $T_m(I)$ is falling ($214\text{A} \lesssim I \lesssim 360\text{A}$). The Joule heating voltage U_J

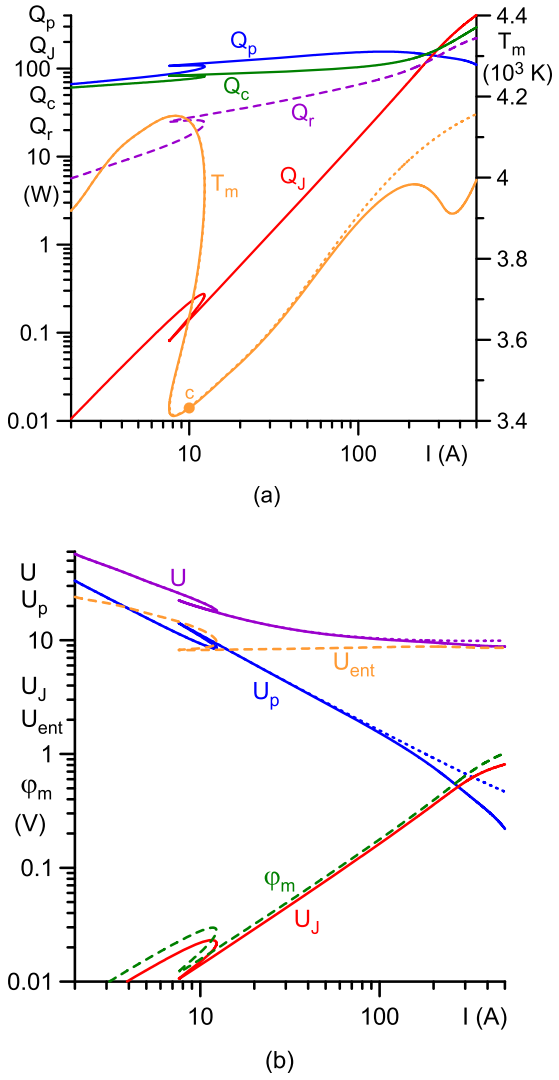

FIG. 6. (a) Thermal balance of the cathode. (b) Energy balance of the near-cathode layer, maximum voltage drop inside the cathode, and volt equivalent of the Joule heating. $p = 1$ bar, cylindrical cathode with a hemispherical tip, $R = 1$ mm, $h = 12$ mm, $T_c = 300$K, mixed mode. Dotted: calculations neglecting Joule heat generation.

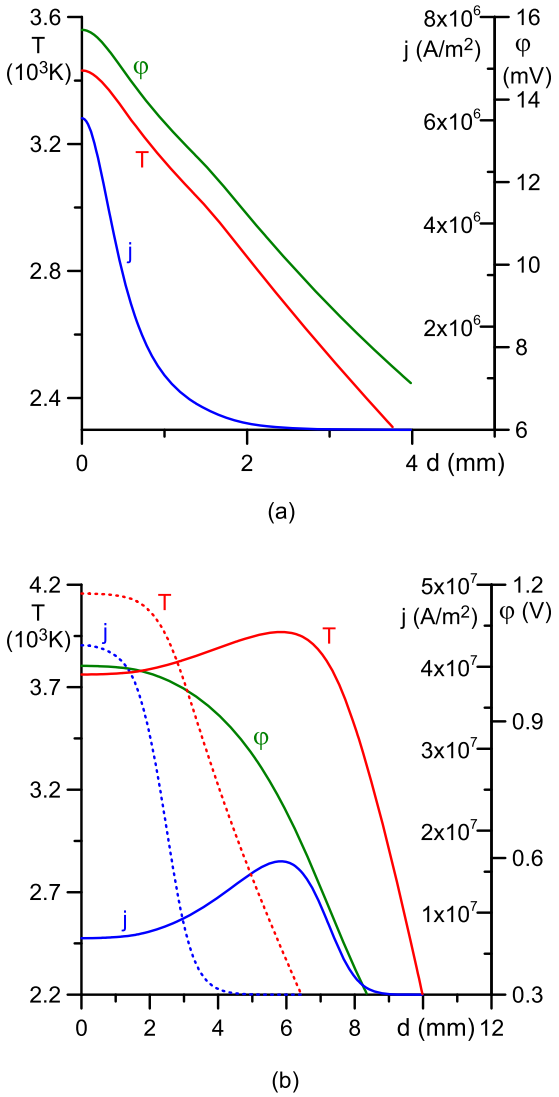

FIG. 7. Distributions of the temperature, the current density, and the potential along the cathode surface. $p = 1$ bar, cylindrical cathode with a hemispherical tip, $R = 1$ mm, $h = 12$ mm, $T_c = 300$K, mixed mode. Dotted: calculations neglecting Joule heat generation. (a): $I = 10$ A. (b): $I = 500$ A.

remains close to the maximum voltage drop inside the cathode, φ_m. Q_J exceeds Q_p, i.e., Joule effect is the main heating mechanism of the cathode, for $I \gtrsim 274$A.

Distributions of temperature, potential and current density along the cathode surface are shown in Fig. 7. [Note that in this figure the range $0 \leq d \leq 1.57$ mm corresponds to the front (spherical) surface of the cathode while the range $d \geq 1.57$ mm corresponds to the lateral (cylindrical) surface.]

Distributions shown in Fig. 7(a) refer to the state c marked in Fig. 6(a); a diffuse-like mode with the whole front surface of the cathode being rather hot. The dotted lines coincide with the solid lines and are not seen, again showing the insignificance of the Joule heating at low currents. The dotted lines in Fig. 7(b) reveal diffuse-like distributions with the arc attachment starting to expand to the lateral surface. The account of Joule heating changes this pattern: the maxima of the surface temperature and the current density are shifted to the lateral surface. The maxima are less pronounced than in the case of the diffuse mode; the front surface of the cathode is not significantly colder than the hottest point of the cathode and collects current.

The maximum of the surface temperature coincides with the absolute maximum of the temperature of the cathode body (to which the data shown in Fig. 6(a) refer) for $I \lesssim 325$A. At higher currents, the absolute maximum occurs on the cathode axis; however, T_m exceeds the highest temperature on the surface by no more than 30 K.

C. Spot mode

In Fig. 8, characteristics of the plasma-cathode interaction are shown for conditions of variant 4, where the current transfer occurs in a mode with a 3 D spot attached at the edge of the front surface of the cathode. A detailed discussion of this mode without account of the Joule effect can be found in Ref. 26; here we only note that this mode is constituted by two branches, a high-voltage branch and a low-voltage branch, separated by a turning point; the spot is hot and well pronounced on the high-voltage branch and is

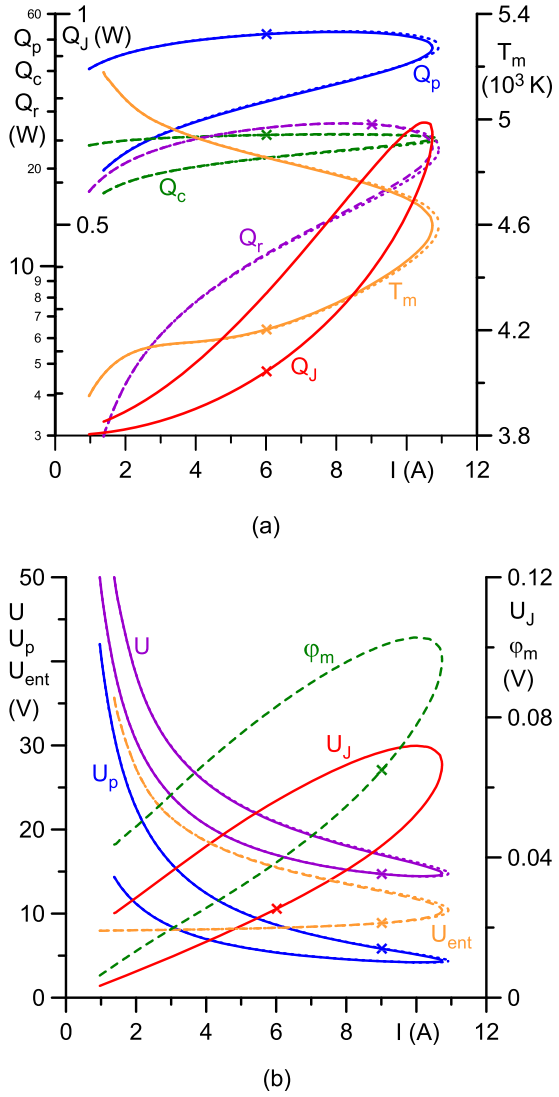

FIG. 8. Characteristics of the plasma-cathode interaction. $p = 2.6$ bar, cylindrical cathode, $R = 0.75$ mm, $h = 20$ mm, $T_c = 300K$, spot mode. Solid and dashed: calculations with account of Joule heat generation. Dotted: calculations neglecting Joule heat generation.

colder and somewhat diffuse on the low-voltage branch. It is the high-voltage branch that is stable and can realize in the experiment;[28] however, the data for the low-voltage branch are also shown here for completeness. In order to distinguish between the two branches, the low-voltage branch of each curve in Fig. 8 is marked by the oblique cross.

One can see from Fig. 8 that, except for a small shift of the turning point in the direction of high currents, Joule heating has virtually no effect on characteristics of the spot mode. It is interesting to note that while on the low-voltage branch the ratio U_p/U decreases with increasing current and the ratio U_{ent}/U increases (a situation similar to the diffuse mode), these ratios remain nearly constant on the high-voltage branch: $U_{ent}/U \simeq 0.7$ and $U_p/U \simeq 0.3$, i.e., about 30% of the energy deposited by the external circuit into the near-cathode layer is transported to the cathode and about 70% is transported into the bulk plasma by the electron current. The Joule heating voltage U_J and the maximum voltage drop inside the cathode, φ_m, vary with the arc current in a similar way, however, the numerical values are not very close in this case.

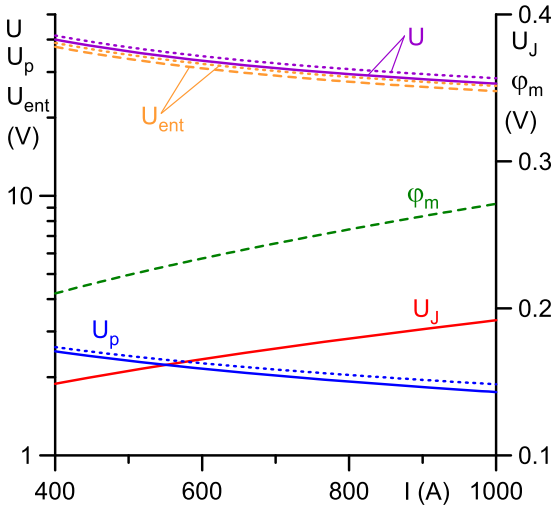

FIG. 9. Energy balance of the near-cathode layer, maximum voltage drop inside the cathode, and volt equivalent of the Joule heating. Solitary spot on an infinite planar cathode. $p = 1$ bar, $T_c = 293$K. Dotted: calculations neglecting Joule heat generation.

In Fig. 9, electrical characteristics of the plasma-cathode interaction are shown for conditions of an axially symmetric solitary spot on an infinite planar cathode. The modelling was performed with the use of an asymptotic boundary condition for the temperature distribution inside the cathode at large distances from the spot which was proposed in Ref. 27. A similar boundary condition was used for the electrostatic potential.

One can see that the effect of Joule heating is negligible, similarly to what happens in the above-treated case of a 3D spot at the edge of a cylindrical cathode. Therefore, the conclusions[27] drawn without account of the Joule effect remain valid. In particular, the contribution of energy transport from the near-cathode layer to the cathode is negligible and practically all the energy deposited by the external circuit into the near-cathode layer is transported into the bulk plasma by the electron current: the ratios U_p/U and U_{ent}/U are nearly constant and equal to 0.06 and 0.94, respectively. The Joule heating voltage U_J and the maximum voltage drop inside the cathode, φ_m, vary with the arc current in a similar way, however, the numerical values differ by about 50%.

IV. DISCUSSION

In all the cases, the maximum voltage drop inside the cathode, φ_m, and, consequently, the volt equivalent of the Joule heating U_J are significantly lower than the near-cathode voltage drop U. Of course, this could have been expected: the considered conditions are not that extreme for the plasma resistance to decrease to values comparable to the resistance of a metallic cathode. On the other hand, a considerable or even most part of the energy deposited into the near-cathode layer is transported by the electron current into the bulk plasma. Therefore, the importance of the Joule effect inside the cathode body is governed by a relation not

between U_J and U but rather between U_J and U_p the volt equivalent of the energy flux from the plasma to the cathode.

At low currents, $U_J \ll U_p$ and the Joule heating is insignificant in all the cases. Since the spot mode on a rod cathode occurs at (relatively) low currents, the Joule heating produces very little effect in this case. In all the other cases, the near-cathode voltage U decreases with increasing current and so does U_p. U_J increases with increasing current and may eventually become comparable to U_p: the Joule heating comes into play. The values of current to rod cathodes at which U_J attains a value equal to that of U_p are shown in Table I. Also shown are corresponding values of U_J and U_p. In the case of solitary spot on a planar cathode, $U_J \ll U_p$ in the whole current range investigated; for the purposes of comparison, values of U_J and U_p for $I = 500$ A are shown in the last row of Table I. Note that there are several values of I at which $U_J = U_p$ in variants 1 and 2 as seen in Figs. 2 and 5; the value shown for each variant in Table I is the lowest one.

The sequence of presentation of data referring to different rod cathodes in Table I is chosen such that the value of current at which $U_J \approx U_p$, shown in the second column, increases. The variation of this value for different cathodes may be understood as follows. Since all rod cathodes are thin, one can estimate their electrical resistance by means of the conventional formula $\Omega = h/\pi\sigma_0 R^2$, where σ_0 is a characteristic electrical conductivity. In the case of a solitary spot, one can use an analytical solution of the Laplace equation describing the distribution of current entering through a circle of radius a a half-space of a constant electrical conductivity σ_0, the current density inside the circle being constant: the potential difference between the center of the circle and infinity is $\Delta\varphi = I/\pi a\sigma_0$ (e.g., Ref. 6). An "effective resistance" of the cathode may be defined as $\Omega = \Delta\varphi/I$ and equals $\Omega = 1/\pi\sigma_0 a$.

Resistances Ω estimated by means of these formulas are shown in Table I. σ_0 was set equal to $2 \times 10^6 \Omega^{-1}\mathrm{m}^{-1}$, which is a representative value for tungsten in the temperature range of interest; a was set equal to 0.6 mm, which is a numerically computed value of the spot radius (position of the first maximum in the distribution over the cathode surface of the energy flux from the plasma[27]) for $I = 500$ A. Also shown in Table I is the voltage drop $I\Omega$. One can see that $I\Omega$ indeed is close to the (calculated numerically) values of U_j. Furthermore, since values of U_p for all rod cathodes are not very different, the current at which the Joule heating comes into play is approximately inversely proportional to Ω. This explains the sequence seen in Table I. In the case of a solitary spot on an infinite cathode, the effective resistance of the cathode is much lower than that of the rod cathodes.

TABLE I. Current values for which Joule heating becomes equal to the plasma heating.

Cathode	I (A)	U_J, U_p (V)	Ω (Ω)	$I\Omega$ (V)
Rod cathode 2	26	0.90	3.5×10^{-2}	0.91
Rod cathode 1	120	0.80	6.8×10^{-3}	0.82
Rod cathode 3	274	0.52	1.9×10^{-3}	0.52
planar	500	0.16, 2.31	2.7×10^{-4}	0.14

Additionally, U_p is higher than that for rod cathodes (which is due to a significantly lower thermal resistance). Therefore, it is not surprising that the Joule heating does not come into play in the case of a solitary spot in the whole current range considered.

In the case where the current transfer at low currents occurs in the diffuse mode (rod cathodes 1 and 2), coming into play of the Joule heating is marked by a retrograde behavior of characteristics of the plasma-cathode interaction. States belonging to the retrograde section are unstable; therefore, the retrograde behavior of computed steady-state solutions corresponds to hysteresis in the experiment. There is no such behavior when the Joule heating comes into play in the case of a cathode operating in the mixed mode (rod cathode 3). In both cases, the thermal and electrical regimes of the cathode change dramatically when the Joule heating comes into play: the maximum of the surface temperature and the current density is shifted from the front surface of the cathode to the lateral surface; the maximum temperature T_m of the cathode decreases and there is even a current range where the dependence of T_m on the arc current is decreasing; at very high currents the maximum temperature may occur at the cathode axis rather than on the surface. This dramatic change is unsurprising, giving the different nature of cathode heating by the plasma and due to the Joule effect: surface vs. volume heating. The retrograde behavior which may accompany Joule heating coming into play also is unsurprising, since interaction of strongly nonlinear effects may be quite nontrivial.

For currents high enough (exceeding 271 A, 70 A, and 274 A for the variants 1, 2, and 3, respectively), Joule effect is the main mechanism of heating of rod cathodes.

In the case of rod cathodes operating in the diffuse and mixed modes, the variation of potential of the cathode surface within the arc attachment is not very considerable, also where the Joule effect is significant. As a consequence, one can introduce a parameter equal to the potential difference between the arc attachment and the base of the cathode and term this parameter the voltage drop inside the cathode, and this parameter will govern the Joule heating of the cathode, $U_J \approx \varphi_m$. Another consequence is that if one wants to take into account a variation of potential inside the cathode body while considering the whole system arc-electrodes, this would result in a shift of potential of the current-collecting cathode surface with respect to the base by a certain voltage which, in addition to being small compared to the near-cathode voltage drop, is constant within the arc attachment.

In Ref. 4, the measured distribution of surface temperature was reported for cylindrical cathodes with a conical tip with cone angles from 12° to 60°. The cathodes were made of thoriated tungsten and the arc operated at the current $I = 200$ A in atmospheric-pressure argon. An off tip maximum in the temperature distribution, similar to those described above in the cases of the diffuse and mixed modes on rod cathodes, was observed on cathodes with a cone angle of 12°. In order to simulate the experiments,[4] in this work modelling has been performed of cylindrical cathodes made of thoriated tungsten with a conical tip with 12° and 60° cone angles, $R = 1.6$ mm, $h = 30$ mm. Skipping calculation data

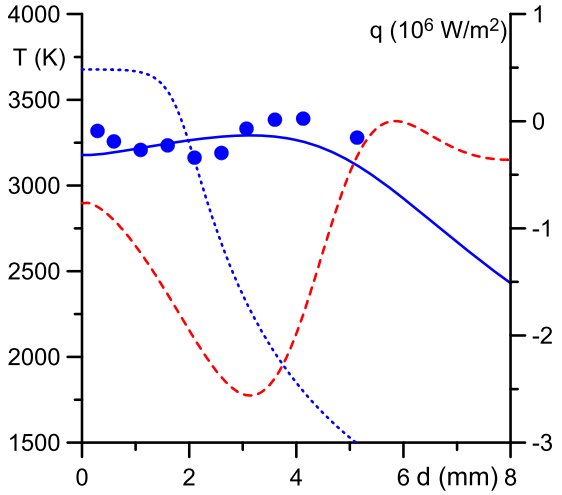

FIG. 10. Distributions along the cathode surface of the temperature (solid) and density of energy flux from the plasma (dashed). Dotted: temperature distribution calculated neglecting Joule heat generation. $p = 1$ bar, thoriated-tungsten cathode with a conical tip. $I = 200$ A. Circles: experimental data on the cathode temperature distribution taken from Ref. 4.

for the cone angle of 60°, we note only that the maximum of the temperature in the modelling occurs at the cathode tip, in agreement with the experiment. Results for the case of 12° are shown in Fig. 10. One can see that calculated temperature distribution is in a reasonable agreement with the experimental data. Note that the computed near-cathode voltage drop for these conditions is rather low: $U = 6.2$ V.

One can see from Fig. 10 that the computed net density of energy flux from the plasma to the cathode surface is negative at all points of the cathode surface except for a narrow region between $d = 5.5$ mm and $d = 6$ mm where q is very small. In other words, it is the cathode that heats the plasma and not the other way round. The reason is illustrated by Fig. 11, where parameters of the near-cathode layer computed as functions of T_w for $U = 6.2$ V are shown in the relevant temperature range. (Note that parameters of the near-cathode layer as functions of T_w and U are given by the model of near-cathode plasma layer[17] simultaneously with the functions $q_p = q_p(T_w, U)$ and $j = j(T_w, U)$.) Here, q_i and q_e are

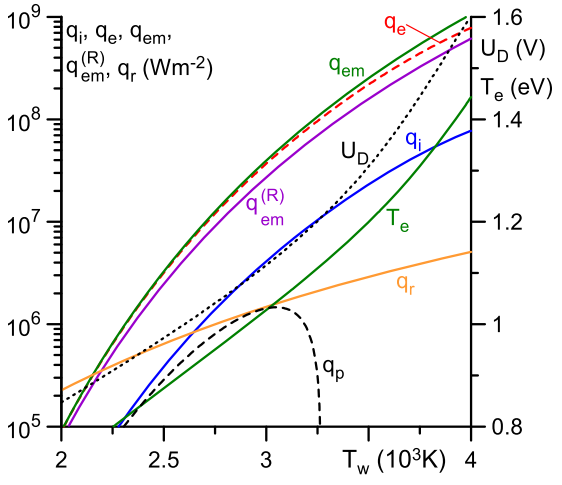

FIG. 11. Characteristics of near-cathode layer. Argon plasma, $p = 1$ bar, thoriated-tungsten cathode, $U = 6.2$ V.

densities of the energy fluxes from the plasma delivered to the cathode surface by the ions and plasma electrons, q_{em} is the density of thermionic emission cooling of the cathode surface, $q_{em}^{(R)} = j_{em}^{(R)} A_f / e$ is the density of thermionic emission cooling evaluated in terms of the density $j_{em}^{(R)}$ of thermionic emission current given by the Richardson formula, T_e is the temperature of plasma electrons in the near-cathode layer, and U_D is the sheath voltage.

One can see from Fig. 11 that the electron temperature varies between approximately 0.9 and 1.2 eV in the cathode surface temperature range of interest (between 2500 K and 3500 K). The sheath voltage is quite low, between 1.0 and 1.3 V. The plasma electron heating q_e significantly exceeds the ion heating q_i. The reason is that the sheath voltage U_D and, consequently, the potential barrier that plasma electrons have to overcome before reaching the cathode are quite low. Thermionic emission cooling q_{em} coincides to the graphic accuracy with, or is slightly greater than, the plasma electron heating q_e. q_{em} is not very different from $q_{em}^{(R)}$; note that the Schottky correction varies between 0.3 eV and 0.9 eV.

Also shown in Fig. 11 are $q_p = q_i + q_e - q_{em}$ the density of net energy flux delivered to the cathode surface by the charged particles and q_r the density of losses of energy by the cathode surface through radiation. q_p is negative for $T_w \gtrsim 3270$K. For lower temperatures, q_p is positive but smaller than q_r (except for a narrow range of T_w in the vicinity of $T_w = 2950$K, where $q_p \approx q_r$). Therefore, $q(T_w, U)$ the net density of energy flux from the plasma to the cathode surface is negative in the temperature range of interest, except in the vicinity of $T_w = 2950$ K, where it is close to zero. This explains why the energy flux is directed into the plasma at all points of the cathode surface.

The computed near-cathode voltage drop, the integral power dissipated in the cathode body due to Joule effect, and the integral power delivered to the cathode by the plasma are compared in Table II for the above-described conical-tip thoriated-tungsten cathode (marked W_{Th}), a conical-tip cathode of the same geometry but made of pure tungsten (marked W), the planar cathode, and rod cathode 3 (a rod cathode with a hemispherical tip). The sequence of presentation of data referring to different cathodes is chosen such that the value of the near-cathode voltage U decreases.

One can see that the decrease of U for cathodes made of pure tungsten is accompanied by an increase of contribution of Joule heating, from negligible for the planar cathode to dominating for the conical-tip cathode. The physical meaning of this result is clear. Simple estimates show that if the cathode is heated by energy flux from the plasma, then

TABLE II. The near-cathode voltage drop, the integral power dissipated in the cathode body due to Joule effect, and the integral power delivered to the cathode by the plasma. $I = 200$ A.

Cathode	U (V)	Q_J (W)	Q_p (W)
Planar	57.7	28.3	646.3
Rod cathode 3	9.5	71.6	152.0
Conical tip, W	8.9	166.0	36.5
Conical tip, W_{Th}	6.2	120.7	17.4

fraction of the ion current at the cathode surface is of the order of several tens of per cent [Ref. 1, Sec. 2.2]. Ion current that high cannot come from the bulk plasma [Ref. 1, Sec. 2.2] and is generated in the near-cathode layer. The latter requires a significant electrical power to be deposited into the space-charge sheath. Hence, U_D has to be sufficiently high in the case of a cathode heated by energy flux from the plasma. If, however, the cathode is heated by Joule effect in the cathode body, then the above reasoning is inapplicable and U_D need not be high.

One can see from Table II also that the near-cathode voltage drop on the thoriated-tungsten conical-tip cathode is significantly lower than the voltage on the similar pure-tungsten cathode. One can conclude that very low values of the sheath voltage U_D computed for the thoriated-tungsten cathode are due to both cathode energy balance being dominated by the Joule heating and low work function of the cathode material.

Previously, cathode temperature distributions with an off tip maximum similar to that observed in the experiment[4] have been computed in Refs. 29 and 30. The models[29,30] employ the assumption of LTE (local thermodynamic equilibrium) and neglect the near-cathode space-charge sheath. This approach is strongly different from the one in which the sheath is of central importance and which is used in this and other works (e.g., review Ref. 1; Refs. 9, 11–13, and 31 may be cited as further examples). The two approaches have been compared in Ref. 12 on an example of a 1 cm-long free-burning atmospheric-pressure argon arc under experimental conditions.[15] The arc voltage predicted by a sheath-accounted model was found to exhibit a variation with the arc current similar to the one revealed by the experiment; it exceeds the experimental values by no more than approximately 2 V in the current range of 20–175 A. About two thirds or more of the arc voltage is contributed by the near-cathode layer. On the other hand, it was found that the LTE approach overestimates both the resistance of the bulk of the arc column and the resistance of the part of the column that is adjacent to the cathode, and this overestimation may compensate, or not, neglect of the voltage drop in the near-cathode sheath.

The modelling[12] neglected the Joule heating in the cathode body. Results obtained in this work on the rod cathode 3 (which was the one employed in the experiments[15] and simulated in Ref. 12) justify such approach: one can see from Fig. 6 that the effect of Joule heating for $I \lesssim 200$A is rather weak. On the other hand, in cases where the Joule heating is dominating and the cathode is made of thoriated tungsten or other material with a low work function, the space-charge sheath voltage may be quite low.

The latter cases are difficult for modelling. On one hand, the presence of a sheath affects the electron current coming to the cathode from the plasma and the electron emission current even if the sheath voltage is quite low, and this renders the use of LTE models problematic. On the other hand, the use of the model of nonlinear surface heating, which assumes a sheath with a significant voltage drop, is problematic as well. It seems that one should think of an approach combining a model of the near-cathode sheath with a two-temperature chemically non-equilibrium model of quasi-neutral plasma, similar to the one developed in the recent work.[13] Leaving this question beyond the scope of this work, we note only that since energy flux coming from the plasma is not decisive in such cases, both the approach[29,30] and the present approach may be qualitatively correct as far as the cathode temperature distribution is concerned. For example, both approaches correctly describe the off tip maximum of the cathode surface temperature.

V. CONCLUSIONS

The model of nonlinear surface heating can be extended to take into account the Joule effect inside the cathode body. The Joule heating has virtually no effect in the cases of a spot mode on a rod cathode and of a solitary spot on an infinite cathode. In the cases of a diffuse and mixed modes on rod cathodes, the Joule heating is a minor effect at low currents but becomes important as the current increases. Variation of the current value at which this happens for cathodes of different shapes, and also the fact that Joule heating plays no role for spots on an infinite cathode, can be understood by means of simple considerations involving the electrical resistance of rod cathodes or effective resistance of the infinite planar cathode. Coming into play of the Joule heating is in some cases accompanied by a retrograde (hysteresis) behavior of characteristics of the plasma-cathode interaction and in all cases causes a dramatic change of thermal and electrical regimes of the cathode: the maximum of the surface temperature and the current density is shifted from the front surface of the cathode to the lateral surface; the maximum temperature T_m of the cathode becomes lower and there is even a current range where the dependence of T_m on the arc current is decreasing; for very high currents, the maximum temperature may occur at the cathode axis rather than on the surface.

One can hope that the approach developed will be useful also in analysis of cathode spots in vacuum arcs, of particular interest being the question at to whether the phenomenon of thermal runaway, predicted by an approximate analytical solution,[7,8] is confirmed by numerical calculations.

ACKNOWLEDGMENTS

This work was performed under the auspices of the projects of FCT—Fundação para a Ciência e a Tecnologia of Portugal PTDC/FIS-PLA/2708/2012 Modelling, understanding, and controlling self-organization phenomena in plasma-electrode interaction in gas discharges: from first principles to applications and PEst-OE/MAT/UI0219/2011 Centro de Ciências Matemáticas.

[1]M. S. Benilov, J. Phys. D: Appl. Phys. **41**(14), 144001 (2008).
[2]R. Bötticher and W. Bötticher, J. Phys. D: Appl. Phys. **33**(4), 367 (2000).
[3]R. Bötticher and W. Bötticher, J. Phys. D: Appl. Phys. **34**(7), 1110 (2001).
[4]J. Haidar and A. J. D. Farmer, J. Phys. D: Appl. Phys. **28**(10), 2089 (1995).
[5]X. Zhou, B. Ding, and J. V. R. Heberlein, IEEE Trans. Compon., Packag. Manuf. Technol., Part A **19**(3), 320 (1996).
[6]J. A. Rich, J. Appl. Phys. **32**(6), 1023 (1961).
[7]E. Hantzsche, IEEE Trans. Plasma Sci. **11**(3), 115 (1983).
[8]E. Hantzsche, IEEE Trans. Plasma Sci. **31**(5), 799 (2003).

[9]A. Bergner, M. Westermeier, C. Ruhrmann, P. Awakowicz, and J. Mentel, J. Phys. D: Appl. Phys. **44**(50), 505203 (2011).
[10]H.-P. Li and M. S. Benilov, J. Phys. D: Appl. Phys. **40**(7), 2010 (2007).
[11]J. J. Gonzalez, F. Cayla, P. Freton, and P. Teulet, J. Phys. D: Appl. Phys. **42**(14), 145204 (2009).
[12]M. S. Benilov, L. G. Benilova, H.-P. Li, and G.-Q. Wu, J. Phys. D: Appl. Phys. **45**(35), 355201 (2012).
[13]M. Baeva, R. Kozakov, S. Gorchakov, and D. Uhrlandt, Plasma Sources Sci. Technol. **21**(5), 055027 (2012).
[14]T. Hartmann, K. Günther, S. Lichtenberg, D. Nandelstädt, L. Dabringhausen, M. Redwitz, and J. Mentel, J. Phys. D: Appl. Phys. **35**(14), 1657 (2002).
[15]N. K. Mitrofanov and S. M. Shkol'nik, Tech. Phys. **52**(6), 711 (2007).
[16]A. Bauer and P. Schultz, Z. Phys. **139**(2), 197 (1954).
[17]M. S. Benilov, M. D. Cunha, and G. V. Naidis, Plasma Sources Sci. Technol. **14**(3), 517 (2005).
[18]Y. S. Touloukian, R. W. Powell, C. Y. Ho, and P. G. Clemens, *Thermal Conductivity, Metallic Elements and Alloys,* Thermophysical Properties of Matter Vol. 1 (IFI/Plenum, New York-Washington, 1970).
[19]S. W. H. Yih and C. T. Wang, *Tungsten: Sources, Metallurgy, Properties, and Applications* (Plenum, New York, 1979).
[20]G. K. White and M. L. Minges, Int. J. Thermophys. **18**(5), 1269 (1997).
[21]R. Morrow and J. J. Lowke, J. Phys. D: Appl. Phys. **26**(4), 634 (1993).
[22]J. Luhmann, D. Nandelstädt, A. Barzik, and J. Mentel, in *Proceedings, Contributed Papers, XXIV International Conference on Phenomena in Ionized Gases*, edited by P. Pisarczyk, T. Pisarczyk, and J. Wolowski (Institute of Plasma Physics and Laser Microfusion, Warsaw, 1999), vol. 1, pp. 13–14.
[23]L. Dabringhausen, O. Langenscheidt, S. Lichtenberg, M. Redwitz, and J. Mentel, J. Phys. D: Appl. Phys. **38**(17), 3128 (2005).
[24]M. S. Benilov, M. D. Cunha, and M. J. Faria, J. Phys. D: Appl. Phys. **42**(14), 145205 (2009).
[25]M. S. Benilov and M. D. Cunha, J. Phys. D: Appl. Phys. **35**(14), 1736 (2002).
[26]M. S. Benilov, M. Carpaij, and M. D. Cunha, J. Phys. D: Appl. Phys. **39**(10), 2124 (2006).
[27]M. S. Benilov and M. D. Cunha, J. Phys. D: Appl. Phys. **36**(6), 603 (2003).
[28]M. S. Benilov and M. J. Faria, J. Phys. D: Appl. Phys. **40**(17), 5083 (2007).
[29]J. J. Lowke, R. Morrow, and J. Haidar, J. Phys. D: Appl. Phys. **30**(14), 2033 (1997).
[30]J. Haidar, J. Appl. Phys. **84**(7), 3518 (1998).
[31]F. Cayla, P. Freton, and J.-J. Gonzalez, IEEE Trans. Plasma Sci. **36**(4), 1944 (2008).